Cement & Concrete Composites 44 (2013) 9–16

Contents lists available at ScienceDirect

Cement & Concrete Composites

journal homepage: www.elsevier.com/locate/cemconcomp

Influence of damage in the acoustic emission parameters

A. Carpinteri [a], G. Lacidogna [a], F. Accornero [a], A.C Mpalaskas [b], T.E. Matikas [b], D.G. Aggelis [c,*]

[a] Department of Structural, Geotechnical and Building Engineering, Politecnico di Torino, Italy
[b] Department of Materials Science and Engineering, University of Ioannina, 45110 Ioannina, Greece
[c] Department of Mechanics of Materials and Constructions, Vrije Universiteit Brussel, Pleinlaan 2,1050 Brussels, Belgium

ARTICLE INFO

Article history:
Received 31 May 2012
Received in revised form 17 May 2013
Accepted 1 August 2013
Available online 14 August 2013

Keywords:
Acoustic emission
Signal attenuation
Frequency content
Cracking mode
Damage domain
Energy density approach
b-Value analysis

ABSTRACT

Acoustic emission (AE) is a Non Destructive Inspection Technique, widely used for monitoring of structural condition of different materials like concrete, masonry and rock. It utilizes the transient elastic waves after each fracture occurrence, which are captured by sensors on the surface. Several parameters of the AE behavior enlighten the damage stage within the material. These may be the cumulative AE activity, which is connected to the density of cracks and the emission energy which is connected to the cracks' intensity. Additionally, AE waveform parameters like duration and frequency content depend on the motion of the crack tip and therefore, carry information about the mode of the crack. Study of the AE indices enlightens the fracture process, enabling predictions on the remaining life. However, the experimental conditions crucially affect the waveforms captured by the sensors. Specimen size, as well as sensor type and sensors separation distance exercise strong influence in the acoustic emission parameters. Since AE features like amplitude and energy are used for characterization purposes in the framework of an energy density approach and frequency is used in cracking mode classification schemes, the influence of the above mentioned experimental parameters should be certainly taken into account in order to lead to more accurate results and increase reliability. This would help to expand the use of AE in situ which so far is hindered by geometric and other technical reasons that allow only a case-specific approach. In the present paper fracture experiments in different specimen sizes of cementitious and rock materials are described while the sensor location relatively to the cracking zone is altered. The aim of this study is to validate the use of cracking characterization in laboratory and check the extension for similar schemes in real size structures with a multiscale methodology.

© 2013 Elsevier Ltd. All rights reserved.

1. Introduction

Acoustic emission (AE) is a nondestructive monitoring method which takes advantage of the elastic energy after crack propagation events [1]. The micro-motion of the tip of the crack excites elastic waves which are acquired by sensors on the surface of the material. The number of recorded signals during loading is connected to the number of active sources within the material [2,3]. Additionally, the signals depend on their source, and specifically the intensity and the mode of fracture. Therefore, the number of recorded hits and key waveform features like amplitude, energy and frequency carry information from the damage mode and the fracture process [4–7]. In general, tensile mode of failure generally develops before shear [8]; therefore, the characterization of cracks as to their mode provides a warning before failure. The received wave depends on the motion of the crack tip, as well as on the orientation of the crack relatively to the receivers and the distance between the cracking source and the sensor. When a cracking event occurs, all possible wave modes (longitudinal, transverse and Rayleigh if the crack is surface breaking) are excited. A tensile cracking incident (Fig. 1) excites most of the energy in the form of longitudinal waves. Therefore, most of the energy arrives in the initial part of the acquired waveform since longitudinal waves are the fastest type. When shear cracking occurs, the percentage of energy emitted in the shear wave mode is increased resulting in a delay of the main energy cycles of the waveform. This leads in a long rise time (RT), and quite low rise angle of the waveform, see Fig. 1 [8,9]. AE duration is the time delay between the first and last threshold crossings. Amplitude, *A* is the maximum voltage of the waveform, as seen again in Fig. 1 and "AE energy" is the area under the rectified signal envelope. Some frequency features of interest, derived after fast Fourier transformation of the signals are the central frequency (CF) and the peak frequency (PF). Central frequency is the centroid of the spectrum while PF is the frequency with the highest magnitude [10].

The applicability of the above mentioned points depends on the geometric conditions, orientation of the cracks and the heterogeneity of the medium. In laboratory scale, it has been shown that

* Corresponding author. Tel.: +32 2 629 3541; fax: +32 2 629 2928.
E-mail addresses: daggelis@vub.ac.be, daggelis@cc.uoi.gr (D.G. Aggelis).

0958-9465/$ - see front matter © 2013 Elsevier Ltd. All rights reserved.
http://dx.doi.org/10.1016/j.cemconcomp.2013.08.001

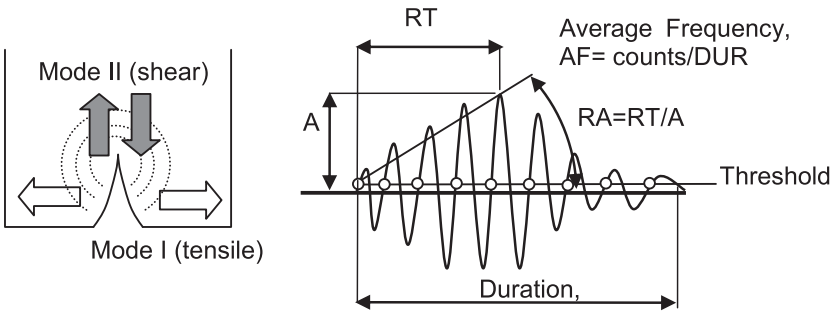

Fig. 1. Cracking modes and typical AE signals.

damage characterization can be conducted with relative success [8,9,11]. As an example taken from recent experimental projects [9], Fig. 2 shows the PF of the AE hits during bending of steel fiber reinforced concrete beams. While load is increasing to the maximum value of 12 kN the majority of the AE hits exhibits PF values mainly between 400 and 500 kHz. At the moment of load drop and thereafter several hits exhibit PF lower than 400 kHz. This behavior has been attributed to the different fracture mechanisms dominating the pre-peak and the post-peak loading stages. Before load drop, AE events are due to the tensile matrix micro-cracking. After the main crack formation, fiber pull-out is also an active mechanism. This leads to emission of signals with much broader frequency content, even below 100 kHz. The solid line that represents the moving average of recent 40 hits starts at approximately 400 kHz before main fracture, while later it fluctuates between 200 and 300 kHz. From this simple example it can be concluded that the different mode of fracture (tensile cracking and shear pull-out) have different AE signatures. Similar examples and conclusions are available in recent literature [8,9,12–15] showing that damage characterization is possible especially in laboratory specimens. However, the expansion of the laboratory criteria to real structures is not easy mainly due to geometry factors and the texture of the material [16]. These factors prevent from general application and make the combined study of AE and elastic wave propagation necessary in an effort to quantify the distortion effect on the waveform features. As any other monitoring methodology, AE provides some deterministic information and some measurements subject to correct interpretation. Specifically for AE, the number of "events" can be specifically combined with the number of cracking incidents. However, the received energy or frequency strongly depend on a number of parameters that may cause ambiguity as to the original source.

The reasons are related among others to the measuring system, i.e. mainly level of sensitivity and frequency response of the sensors. This is the reason that standardization is attempted recently [8]. Additionally the texture of the material is important. Different materials exhibit different wave propagation properties (mainly attenuation and velocity) which distort the wave away from its original shape. The shape and size of the structure is also important since reflections at the boundaries and plate geometries induce further distortion. This is enhanced by the presence of damage in the form of micro-cracks which increase scattering. Finally, a very important factor is the distance between the cracking source and the monitoring point. As the distance increases, the effect of distortion is accumulated resulting in poor characterization efficiency in case of large dimension structures.

An example of the aforementioned distortion is shown in Fig. 3 where the waveforms at three different positions on a fiber reinforced mortar plate specimen is shown. The waveforms despite the relatively small distances between the sensors (less than 80 mm from the source, see embedded schematic image) exhibit strongly different characteristics in amplitude, rise time and frequency components. The obvious change in the shape of the waveform is due to the combined effect of: (i) plate wave dispersion which leads to the separation of plate wave modes propagating with different velocities (high frequency first, low frequency trailing), (ii) scattering on the heterogeneous texture of fibre mortar, (iii) damping of the constituents and of course and (iv) different propagation distance.

In the present paper mortar specimens are fractured in three point bending and the AE behavior is recorded by two sensors at different distances from the crack. The results show that the change in the waveform features is quite strong in terms of frequency and energy and should not be neglected from any characterization approach.

As it emerges from the previous discussion, attenuation properties of AE waves in inhomogeneous materials such as mortar and concrete – but this concept can also be easily extended to other

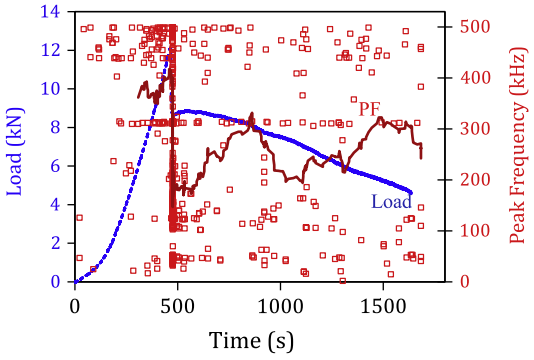

Fig. 2. Load history and peak frequency of AE signals.

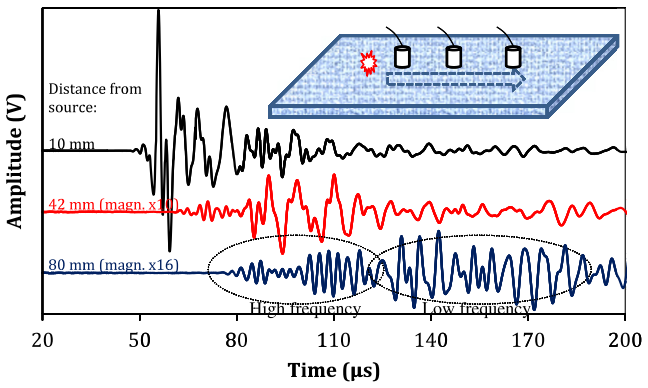

Fig. 3. Waveforms received by Pico sensors on a fiber-reinforced mortar plate of 2 mm thickness.

quasi-brittle materials like rocks – influence critical AE parameters. Hence, taking into account the attenuation and distortion phenomena in the travel path between the source of the signal and the sensor, in order to apply these theories it should be ensured that the measuring system is able to detect the most relevant AE events reflecting the cracking process of the material. Higher frequency components propagate in quasi-brittle materials with a greater attenuation. Based on experimental results on mortar and concrete, if the wavelength is larger than the maximum inhomogeneity, the wave "passes over" without significant modifications in its waveform [17]. In general, for a measuring area at a distance of several meters from the sensor, only AE waves with frequency components lower than 100 kHz are detectable. Therefore, the employed AE sensors, and the volume of material analyzed should take into account these limitations. In other words, it is necessary to employ broadband or resonant sensors, with the right amplification, depending on the size and the damage level of the monitored structure [1].

Starting from these considerations, two different approaches are proposed to obtain indirect estimation of the physical fractal dimension of the damage domain up to the peak load of quasi-brittle materials, such as concrete and rocks, mainly subjected to compression. First, an energy density approach is presented, based on the size-effects of the energy release determined by the AE technique. This calculation is performed by considering specimens with different size-scale. Then, a complementary method is proposed, based on the *b*-value analysis of AE events [18]. Since the *b*-value is size-independent, its evaluation evidences the similarity between the damage process in a structure and the seismic activity in a region of the Earth crust [18].

2. Energy density criterion

Acoustic emission data have been interpreted by means of statistical and fractal analysis, considering the multiscale aspect of cracking phenomena [19]. This approach has shown that the energy release, detected by AE, occurs in a fractal (lacunar) domain with a dimension lower than 3.0. Consequently, a multiscale criterion to predict the damage evolution has been formulated. Recent developments in fragmentation theories [20], have shown that the energy W during microcrack propagation is released over a fractal domain comprised between a surface and the specimen volume V. As a result, the following size-scaling law has been assumed for the energy release W during fragmentation:

$$W \propto V^{D/3}, \tag{1}$$

where D is the so-called fractal exponent, comprised between 2.0 and 3.0. There are numerous evidences on the dependence of the fractal exponent D from the conditions of fragmentation. Catastrophic failure under compression would be associated to low D values approaching to 2.0, whereas extensive crushing under compression would generate higher D values, close to 3.0 [21].

As a consequence of Eq. (1), the energy density scales as:

$$\Psi = \frac{W}{V} \propto V^{(D-3)/3}. \tag{2}$$

This implies that not the true energy density but a fractal energy density (having non-integer physical dimensions).

$$\Gamma = \frac{W}{V^{D/3}}, \tag{3}$$

can be considered as the size-independent parameter.

On the other hand, during microcrack propagation, AE can be clearly detected. The energy release W is proportional to the number N of AE events. Accordingly to the energy release from a fractal domain, as described by Eq. (3), the number of AE events, N, not over a volume but over a fractal domain, can be considered as the size-independent parameter:

$$\Gamma_{AE} = \frac{N}{V^{D/3}}, \tag{4}$$

where Γ_{AE} is the value of AE events fractal density. The fractal criterion in Eq. (4) permits to extend Eq. (1) as follows:

$$W \propto N \propto V^{D/3}. \tag{5}$$

2.1. Experimental assessment

The experimental validation of the theoretical conjecture herein considered is performed on the basis of the results of uniaxial compression tests carried out on cylindrical concrete and rock specimens. The concrete samples were drilled from two pilasters sustaining a viaduct along an Italian highway built in the 1950s [19]. Three different specimen diameters d in a scale range 1.0:2.1:3.4 (d = 27.7, 59.0 and 94.0 mm) and three different slendernesses, $\lambda = h/d$, equal to 0.5, 1.0 and 2.0 were considered. The nine geometries are presented in Fig. 4a. The tests were performed under displacement control, assuming a displacement rate equal to 10^{-4} mm/s, in order to obtain slow crack growth and to detect all possible AE signals. The load was applied by means of rigid steel platens without friction-reducing systems.

The second experimental campaign herein considered concerns the compression tests carried out on rock samples taken from one pillar of the Cathedral of Syracuse, in Sicily. They were drilled from removed elements replaced by other blocks during restoration works. The pillars of the Cathedral have the peculiar interest that they had been obtained by cutting out the stonework walls of the internal cell of the 5th Century B.C. Greek temple of Athena. In the 6th Century, it was transformed into a Catholic Church, and then frequently modified until the present configuration. More in detail, the ancient stone used in the construction of the temple was a calcareous stone located in the area of Plemmirio, just south of Syracuse. Specimens with diameters d in a scale range 1:2:4 (d = 30, 60 and 120 mm), and slenderness $\lambda = 1$, were tested (Fig. 5a). The specimens were subjected to laboratory compressive tests at constant displacement rate of 4×10^{-4} mm/s and monitored by the AE technique [22]. The load was applied by means of rigid steel platens without friction-reducing systems. The results evidenced an average compressive strength equal to 8.20 MPa, with variations due to statistics rather than to clear size-effects.

For all the tested specimens, the number of AE was evaluated in correspondence to the peak stress σ_c, and, in the following, referred to as N_{max}. This analysis is performed by a measuring system counting the events that exceed a certain voltage threshold measured in volts. On average, compression tests show an increase in AE cumulative events number by increasing the specimen volume, as shown in Figs. 4b and 5b. Subjecting the average experimental data to a regression analysis, the parameter D in Eq. (4) can be quantified. The parameter $D/3$ represents the slope, in the bi-logarithmic diagram, of the curve that relates N_{max} to the specimen volume. From the best-fitting, values of $D/3$ equal to 0.766 and 0.779 were obtained for concrete and rocks specimens, respectively (see Figs. 4b and 5b). The corresponding fractal exponents, D, result to be comprised between 2.29 and 2.33. The goodness of fit for the best-fitting curve in Fig. 4b is r^2 = 0.88, while in Fig. 5b is r^2 = 0.99.

3. Statistical distribution of AE events

A statistical interpretation to the variation of the *b*-value during the evolution of damage detected by AE has been proposed, which

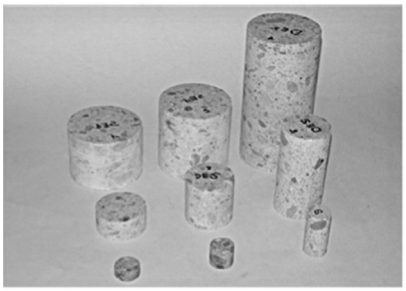

(a) Geometry of the concrete specimens

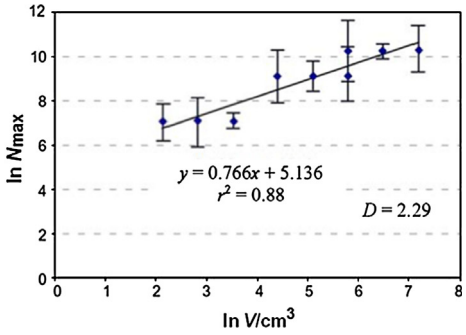

(b) Volume-effect on N_{max}

Fig. 4. Concrete specimens tested by Carpinteri et al. [19].

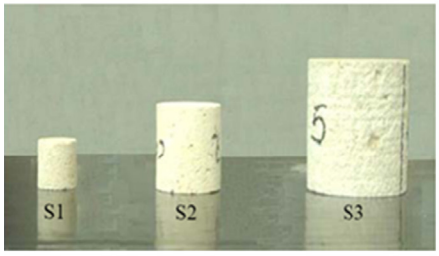

(a) Geometry of the rock specimens

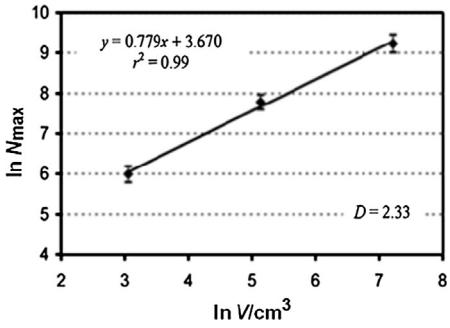

(b) Volume-effect on N_{max}

Fig. 5. Rock specimens tested by Carpinteri et al. [22].

is based on a treatment originally proposed by Carpinteri and co-workers [10,22,23]. The proposed model captures the transition from the condition of diffused criticality to that of imminent failure localization.

By analogy with seismic phenomena, in the AE technique the magnitude may be defined as follows:

$$m = \mathrm{Log}_{10} A_{max} + f(r), \tag{6}$$

where A_{max} is the amplitude of the signal expressed in volts, and $f(r)$ is a correction taking into account that the amplitude is a decreasing function of the distance r between the source and the sensor.

In seismology the empirical Gutenberg–Richter's law [24]:

$$\mathrm{Log}_{10} N(\geqslant m) = a - bm, \quad \text{or } N(\geqslant m) = 10^{a-bm}, \tag{7}$$

expresses the relationship between magnitude and total number of earthquakes in any given region and time period, and it is one of the most widely used statistical relations to describe the scaling properties of seismicity. In Eq. (7), N is the cumulative number of earthquakes with magnitude $\geqslant m$ in a given area and within a specific time range, whilst a and b are positive constants varying from a region to another and from a time interval to another. Eq. (7) has been used successfully in the AE field to study the scaling laws of AE wave amplitude distribution. This approach evidences the similarity between structural damage phenomena and seismic activities in a given region of the Earth's crust, extending the applicability of the Gutenberg–Richter's law to Structural Engineering. According to Eq. (7), the b-value changes systematically at different times in the course of the damage process and therefore can be used to estimate damage evolution modalities.

Eq. (7) can be rewritten in order to draw a connection between the magnitude m and the size L of the defect associated with an AE event. By analogy with seismic phenomena, the AE crack size-scaling entails the validity of the relationship:

$$N(\geqslant L) = cL^{-2b}, \tag{8}$$

where N is the cumulative number of AE events generated by source defects with a characteristic linear dimension $\geqslant L$, c is a constant of proportionality, and $2b = D$ is the fractal dimension of the damage domain.

Aki [25] was the first to show that the seismic b-value is related to the fractal dimension D, and that usually $2b = D$. This assumption – and its implication with the damage energy release rate and time dependent mechanisms, both at the laboratory and at the Earth's crust scale – has been also pointed out by Main [26–28]. Moreover, it has been evidenced that this interpretation rests on the assumption of a dislocation model for the seismic source and requires that $2.0 \leqslant D \leqslant 3.0$, i.e., the cracks are distributed in a fractal domain comprised between a surface and the volume of the analyzed region [29–32].

The cumulative distribution (8) is substantially identical to the cumulative distribution proposed by Carpinteri [23], which gives the probability of a defect with size $\geqslant L$ being present in a body:

$$P(\geqslant L) \propto L^{-\gamma}. \tag{9}$$

Therefore, the number of defects with size $\geqslant L$ is:

$$N^*(\geqslant L) = cL^{-\gamma}, \tag{10}$$

where γ is a statistical exponent measuring the degree of disorder, i.e. the scatter in the defect size distribution, and c is a constant of proportionality. By equating distributions (8) and (10) it is found that: $2b = \gamma$. At the collapse, the size of the maximum defect is proportional to the characteristic size of the structure. As shown by Carpinteri and co-workers [11], the related cumulative defect size

distribution (referred to as self-similarity distribution) is characterized by the exponent $\gamma = 2.0$, which corresponds to $b = 1.0$. It was also demonstrated [23] that $\gamma = 2.0$ is a lower bound which corresponds to the minimum value $b = 1.0$, observed experimentally when the load bearing capacity of a structural member has been exhausted.

Therefore, by determining the b-value it is possible to identify the energy release modalities in a structural element during the monitoring process. The extreme cases envisaged by Eq. (5) are $D = 3.0$, which corresponds to the critical conditions $b = 1.5$, when the energy release takes place through small defects homogeneously distributed throughout the volume, and $D = 2.0$, which corresponds to $b = 1.0$, when energy release takes place on a fracture surface. In the former case diffused damage is observed, whereas in the latter two-dimensional cracks are formed leading to the separation of the structural element.

3.1. b-Value analysis

The analysis of the b-value during the compression test was carried out for one of the 59 mm diameter concrete specimens with slenderness equal to 2.0 taken from the pilaster of the Italian highway viaduct and presented in Section 2.1. During the compression test the specimen was monitored by two wide-band AE sensors sensitive on a frequency range comprised between 50 and 500 kHz. By using the AE device, the threshold level for the signals recorded, fixed at 50 μV, was amplified up to 100 mV. The mechanical waves, due to damage, detected by the two sensors generally lead to distinct "hits", that are considered as an "event" when they occur almost simultaneously [8]. Therefore the events amplitude A_{max} (see Eq. (6)) is characterized by the largest amplitude of the two hits.

A schematic representation and photograph of the experimental setup is seen in Fig. 6a. In order to perform this analysis, information about the signal magnitude is required, instead of events counting only. The b-value is the negative gradient of the log-linear AE frequency vs. magnitude diagram and hence it represents the slope of the amplitude distributions [4,33,34]. Compressive load versus time, cumulated event number, and event rate for each second of the testing time are depicted in Fig. 6b. In the load–time diagram of Fig. 6b all the detected AE events are reported, while for the b-value analysis only events with magnitude $m = Log_{10}A_{max}$ greater or equal than 2 are represented.

The load–time diagram was subdivided into three stages: a first stage (t_0, t_1) extending from initial time to peak load, a second stage (t_1, t_2) going from peak load to main shock, as identified by the maximum value of the acoustic emission rate, and a third stage (t_2, t_f) going from main shock to end of the process. The b-values obtained for each stage are shown in Fig. 6c. They range from 1.64 to 1.20. At the beginning of the loading process, the energy release takes place mostly through the formation of microcracks scattered throughout the volume of the material ($b \cong 1.64$, $D \to 3.0$); at the end of the process, instead, the energy release is seen to concentrate into a two-dimensional crack of a size comparable to that of the specimen, which brings about its separation ($b \cong 1.20$, $D \to 2.0$). In particular, the fractal exponent at the peak load obtained through the b-value is strictly connected to the analogous exponent evaluated by means of the energetic approach: D had appeared as comprised between 2.29 and 2.33 (see Figs. 4b and 5b). The latter, indeed, is related to the critical cumulative number of acoustic emission N_{max} at the peak stress σ_c, when the crack formation is not yet so advanced to lead to the complete specimen separation.

The non-perfect matching between the values obtained for the D exponent of a given material is due to the fact that different approaches can lead to underestimate or overestimate some measurements obtained during the tests. As a matter of fact, the damage fractal dimension D, calculated by Eq. (5), is obtained by a best-fitting of the N_{max} values arranged in bi-logarithmic scale for each specimen volume, whereas, the b-values, obtained by Eq. (7) are defined as the log-linear slope of the frequency–magnitude distribution of AE events. The two approaches, therefore, are completely different. Moreover, the b-value analysis takes into account not only the number of AE events, but also their amplitude. Damage, in fact, especially in the pre-peak branch of the load vs. time diagrams, advances with a considerable number of AE events having small amplitudes, that could result – if the statistic is limited to a single specimen – to an overestimation of the fractal domain D. This experimental evidence is also described in the fundamental paper by Lockner et al. [35] in which it is observed that during triaxial compressive tests on granite and sandstone "the b-values for pre-nucleation events are indeed larger than for post-nucleation events, indicating a greater percentage of low amplitude events in the pre-nucleation phase". The direct computation of the fractal dimension D should be performed by geometrical methods like the box-counting [32], which need the "exact" localization of AE sources.

Some applications of the AE fractal damage model, obtained on the basis of the energy density criterion of Eq. (5), are described in [20,36]. Moreover, the evolution of the damage fractal dimension D, assessed by means of the statistical interpretation of b-value variations (Eq. (7)), are described in [11,37,38]. In these papers the fractal models are used for interpreting data obtained at laboratory scale, and on full scale structures.

The above mentioned correlations exhibit a quite high correlation coefficient. However, general use should be very careful since they are obtained by testing with specific experimental conditions. As an example, increasing the volume of the specimen, increases the number of recorded AE signals, due to the larger population of cracking sources; however, it also increases the distance between the source of the events and the sensors, which entails stronger attenuation and distortion with additional influence on the number and the characteristics of the acquired events. It is obvious that this approach, as well as the aforementioned crack classification schemes would definitely benefit by separating or quantifying the effect of the experimental conditions on the final result.

4. Cracking mode classification Approach

Apart from the above discussed energy density approach, the cracking mode classification schemes are based on the extracted features of the received AE waveforms. Simple experiments were conducted to test the effect of sensor location relatively to the cracking event as explained below.

4.1. Experiment

Six mortar specimens were produced. The aggregates consisted of sand with maximum aggregate size 4.75 mm, while water/cement ratio was 0.55 by mass. The density of the water was 2500 kg/m^3 and the absorption was 2.44% respectively. The specimens were cured in water saturated with calcium hydroxide at 23 ± 2 °C for 28 days prior to testing.

The specimens subjected to three-point bending were 40 × 40 × 160 mm in size (Fig. 7). The load was applied at a constant rate and the experiment was stopped at the moment of fracture (load drop). Concerning AE, two broadband sensors (Pico, PAC) were attached to one side of the specimen as seen in Fig. 7. Acoustic coupling was enhanced by roller bearing grease and the sensors were mounted by tape. The first was placed in a horizontal

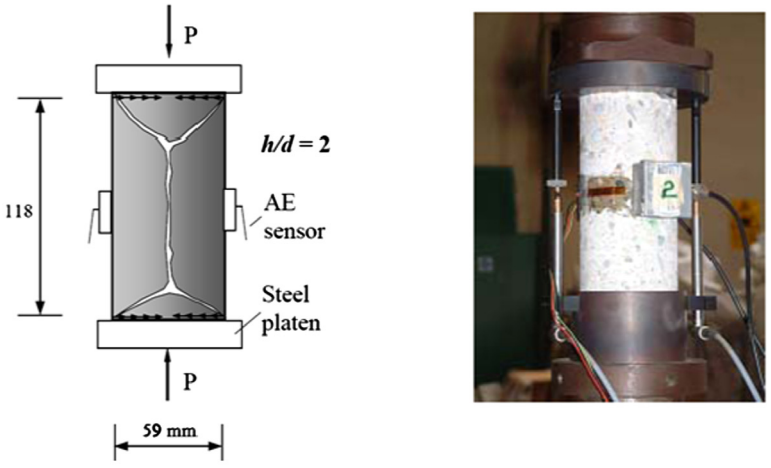

(a) Testing set-up

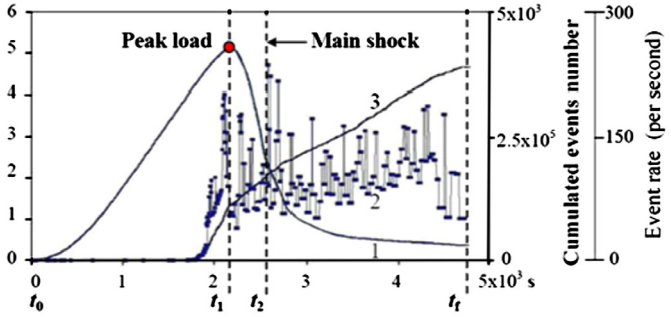

(b) Load 1; Event rate 2; Cumulated events number 3

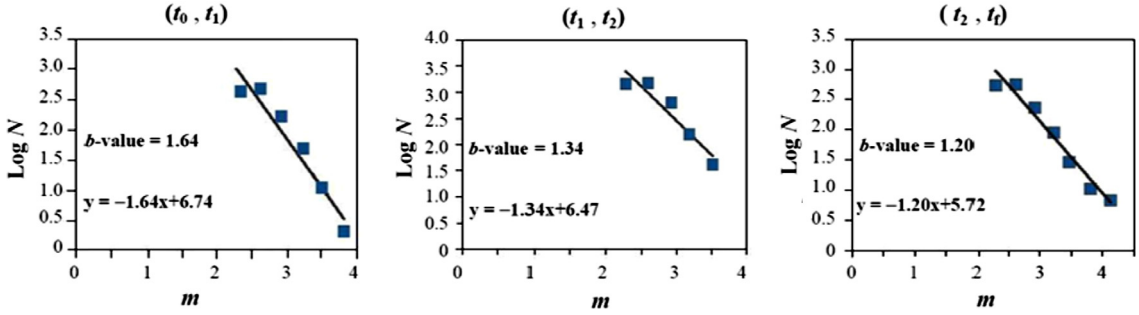

(c) *b*-values

Fig. 6. Cylindrical concrete specimen in compression by Carpinteri et al. [37]: testing set-up, with an AE sensor clearly visible on the lateral surface of the specimen (a); load vs. time diagram and AE activity (b); and *b*-values during the test (c).

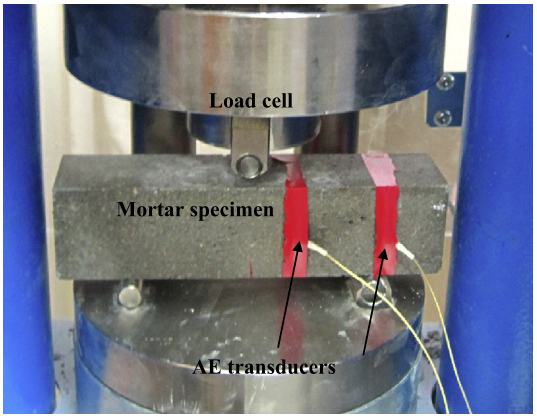

Fig. 7. Experimental setup for three-point bending of mortar with two AE sensors.

distance of 15 mm from the mid-span (point of crack nucleation) and the second at 55 mm, leaving a separation distance of 40 mm between the sensors. Signals above the threshold of 40 dB were recorded in a two-channel monitoring board PCI-2, PAC. Results of five specimens are discussed since one was rejected.

5. Results

When a crack propagation incident occurs this is considered an "AE event". This event leads to a wave that can be recorded by different sensors as distinct "hits". When a cracking event occurs, hits arrive at the different sensors almost simultaneously, with delays that depend on the distance between the source and the sensors. Hence, the determination of an event is usually done automatically as the hits are acquired in real time. Focusing on the AE events increases the reliability of the analysis since it takes into account the hits that were of higher level and captured by more than one

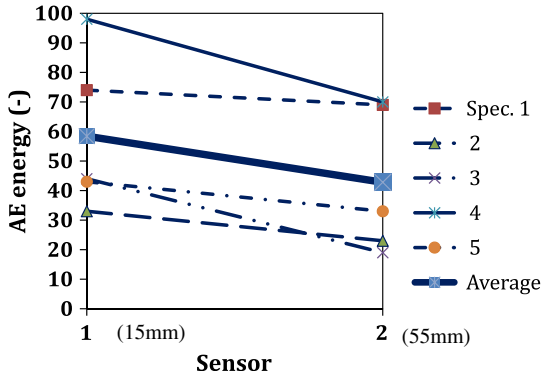

Fig. 8. AE energy for both sensors and different specimens.

transducers. The results presented herein are based on the AE "events". For the whole number of events (typically around 20 for each test), the values of selected AE features were averaged for each sensor. Fig. 8 shows the average energy of the hits for both sensors. It is seen that for the first sensor, the AE energy ranges between 30 and 100 units. The recorded energy at the 2nd sensor ranges from 20 to 70. It is noteworthy that for each one of the five specimens there is a decreasing trend for AE energy between the 1st and 2nd sensor. As an average for the whole number of specimens the energy reduces from 58.4 to 42.8 units between the 1st and 2nd sensor. Therefore, an additional propagation distance of roughly 40 mm reduces the acquired energy by approximately 27%. The reduction seems normal considering attenuation mechanisms. However, the amount of energy drop in such a small distance shows that the specimen size and sensor separation distance are crucial when quantitative AE is undertaken. This implies how important the propagation length is for AE analysis even in laboratory scale.

This aspect of the study, with considerable expansion of the examined population of specimens to several other materials, will be applied in future to obtain reasonable values of the $f(r)$ function of Eq. (6), optimizing the b-value analysis even for large structures.

As aforementioned, frequency features are used for crack mode classification. Therefore, Fig. 9a and b focus on the central and the peak frequency of the hits as monitored by the different sensors. A similar decreasing trend is seen again both for central and peak frequencies. The trends are decreasing and repeatable for each of the specimens. CF decreases by about 11% (from 380 kHz to 340 kHz) between the two sensors. PF which corresponds to the frequency with the maximum magnitude, exhibits more or less the same trend. A strong decrease is noted for all specimens, resulting in an average drop of 23%. This decrease of frequency descriptors is again attributed to the microstructure and mainly scattering of the sand grains, pores and cavities of the cementitious material. Again it is understandable that if a separation distance of 40 mm is responsible for a change of 10–25% in an AE parameter, one should be definitely very careful in application of any laboratory characterization scheme [39] in a real structure.

A final example of distortion of AE signal between the two sensors is included in Fig. 10. There, the duration of the waveforms is depicted for the two sensors and the different specimens. With just one exception (specimen 3) the duration of the signals drops considerably between the two sensors. It is reminded that the duration of an AE waveform is calculated based on a user-defined threshold. When the material is attenuative (like mortar in the present case) it is reasonable that less peaks of the waveform will exceed the threshold level as the wave is propagating away from the source, hence leading to acquisition of shorter waveforms. The average reduction of duration is about 6% from 506 μs to 475 μs. Different

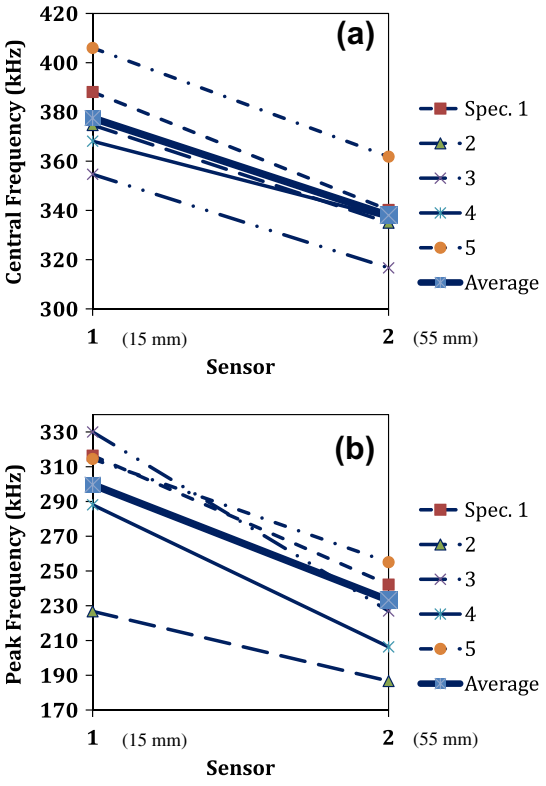

Fig. 9. (a) Central and (b) peak frequency for both sensors and different specimens.

AE characteristics based on the waveform shape exhibit similar change between the two sensors as was reported recently [40].

The three kinds of features (energy-, frequency- and waveform shape-related) that were analyzed in this section show how propagation of a few additional mm attenuates and distorts the signals. The differences between the sensors are quite strong especially taking into account that the two sensors are separated only by 40 mm. This distortion would reduce the accuracy of any crack classification scheme unless the exact experimental conditions are applied. In laboratory, the distance between the cracking source and the sensor is limited due to the limited size of the specimens. Therefore, although the effect of distortion and attenuation is evident, still it does not hinder the establishment of classification rules. However, in real structures the cracking event may occur just a few mm away from the sensor or several meters away. The interchangeable accumulated effect of inhomogeneity that would be different for events coming from different locations would definitely mask the results and make derivation of reliable conclusions troublesome.

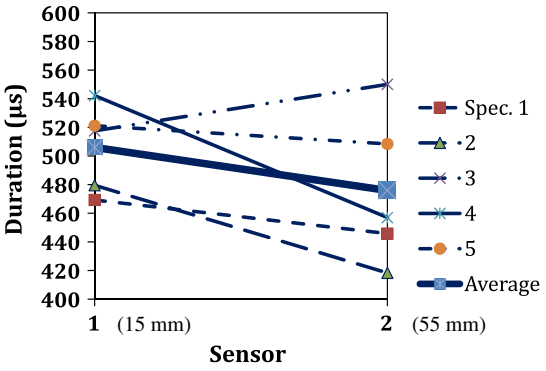

Fig. 10. AE duration for both sensors and different specimens.

The above discussion shows clearly that study of AE should be certainly combined with elastic wave propagation study. This will potentially enable clearing of the sensor-acquired AE waveform from attenuation and distortion leading to features that are closer to the waveform as emitted by the crack. More experiments with multiple sensors and different sizes of specimens are necessary, while three dimensional simulations of wave propagation would certainly help to understand the effect of microstructure not only on classic wave parameters like velocity and attenuation but also on waveform features like duration, or frequency indicators like the ones used in AE.

6. Conclusions

The present study occupies with acoustic emission in materials with microstructure such as cementitious mortar, concrete and rock. Different AE features are used for characterization of fracturing of the materials. These parameters (related mainly to frequency and energy of the waveforms) undergo strong distortion and attenuation due to the heterogeneity of the material. Experiments in mortar specimens show that an additional propagation distance of a few cm affects the calculated values by a large percentage. Therefore, the use of AE waveform features as received by the sensor should be very careful for characterization purposes. Similarly in energy density approaches, the effect of attenuation should be incorporated with detail since a change in the volume of the specimen automatically induces a change in the length of the typical propagation path from the crack to the receiver, which may well affect the sensitive coefficients such as the fractal exponent. The next step would be to quantify the effect of distortion and establish procedures aiming at clearing the acquired AE population from the accumulated distortion.

References

[1] Grosse CU, Ohtsu M. Acoustic Emission Testing. Heidelberg: Springer; 2008.
[2] Carpinteri A, Cardone F, Lacidogna G. Energy emissions from failure phenomena: mechanical, electromagnetic, nuclear. Exp Mech 2010;50:1235–43.
[3] Kurz JH, Finck F, Grosse CU, Reinhardt HW. Stress drop and stress redistribution in concrete quantified over time by the *b*-value analysis. Struct Health Monit 2006;5:69–81.
[4] Shiotani T, Fujii K, Aoki T, Amou K. Evaluation of progressive failure using AE sources and improved *b*-value on Slope Model Tests. Progr Acoust Emiss 1994;7:529–34.
[5] Watanabe T, Hosomi M, Yuno K, Hashimoto C. Quality evaluation of shotcrete by acoustic emission. Construct Build Mater 2010;24:2358–62.
[6] Muralidhara S, Raghu Prasad BK, Eskandari H, Karihaloo BL. Fracture process zone size and true fracture energy of concrete using acoustic emission. Construct Build Mater 2010;24:479–86.
[7] Vidya Sagar R, Raghu Prasad BK, Karihaloo BL. Verification of the applicability of lattice model to concrete fracture by AE study. Int J Fract 2010;161:121–9.
[8] Ohtsu M. Recommendation of RILEM TC 212-ACD: acoustic emission and related NDE techniques for crack detection and damage evaluation in concrete: test method for classification of active cracks in concrete structures by acoustic emission. Mater Struct 2010;43(9):1177–81.
[9] Aggelis DG, Soulioti DV, Gatselou EA, Barkoula N.-M., Matikas TE. Monitoring of the mechanical behavior of concrete with chemically treated steel fibers by acoustic emission. Construct Build Mater. doi: 10.1016/j.conbuildmat.2012.06.066.
[10] Aggelis DG, Matikas TE. Effect of plate wave dispersion on the acoustic emission parameters in metals. Comput Struct 2012;98–99:17–22.
[11] Carpinteri A, Lacidogna G, Niccolini G, Puzzi S. Critical defect size distributions in concrete structures detected by the acoustic emission technique. Meccanica 2008;43:349–63.
[12] Grosse C, Reinhardt H, Dahm T. Localization and classification of fracture types in concrete with quantitative acoustic emission measurement techniques. NDT&E Int 1997;30(4):223–30.
[13] Shiotani T. Evaluation of long-term stability for rock slope by means of acoustic emission technique. NDT&E Int 2006;39(3):217–28.
[14] Farhidzadeh A, Salamone S, Singla P. Probabilistic approach for damage identification and crack mode classification in reinforced concrete structures. J Intelligent Mater Syst Struct. doi: 10.1177/1045389X13484101.
[15] Elfergani HA, Pullin R, Holford KM. Damage assessment of corrosion in prestressed concrete by acoustic emission. Construct Build Mater 2013;40:925–33.
[16] Scholey JJ, Wilcox PD, Wisnom MR, Friswell MI. Quantitative experimental measurements of matrix cracking and delamination using acoustic emission. Composite part A 2010;41:612–23.
[17] Landis EN, Shah SP. Frequency-dependent stress wave attenuation in cement-based materials. J Eng Mech 1995;121:737–43.
[18] Scholz CH. The frequency–magnitude relation of microfracturing in rock and its relation to earthquakes. Bull Seismol Soc Am 1968;58:399–415.
[19] Carpinteri A, Lacidogna G, Pugno N. Structural damage diagnosis and life-time assessment by acoustic emission monitoring. Eng Fract Mech 2007;74:273–89.
[20] Carpinteri A, Pugno N. Fractal fragmentation theory for shape effects of quasi-brittle materials in compression. Mag Concr Res 2002;54:473–80.
[21] Weiss J. Fracture and fragmentation of ice. A fractal analysis of scale invariance. Eng Fract Mech 2001;68:1975–2012.
[22] Carpinteri A, Lacidogna G, Manuello A. The *b*-value analysis for the stability investigation of the ancient Athena temple in Syracuse. Strain 2009;47:e243–53.
[23] Carpinteri A. Scaling laws and renormalization groups for strength and toughness of disordered materials. Int J Solids Struct 1994;31:291–302.
[24] Richter CF. Elementary seismology. San Francisco and London: W.H. Freeman; 1958.
[25] Aki A. A probabilistic synthesis of precursory phenomena. Earthquake prediction: an international review. In: M. Ewing Series, Simpson DW, Richards PG, editors, vol. 4. pp. 566–74.
[26] Main IG. A modified Griffith criterion for the evolution of damage with a fractal distribution of crack lengths: application to seismic event rates and *b*-values. Geophys J Int 1991;107:353–62.
[27] Main IG. Damage mechanics with long-range interactions: correlation between the seismic *b*-value and the two point correlation dimension. Geophys J Int 1992;111:531–41.
[28] Main IG. A damage mechanics model for power-law creep and earthquake aftershock and foreshock sequences. Geophys J Int 2000;142:151–61.
[29] King GCP. The accommodation of large strains in the upper lithosphere of the Earth. Pure Apply Geophys 1983;121:761–815.
[30] Hirata T. A correlation between *b*-value and the fractal dimension of earthquakes. J Geophys Res 1989;94:7507–14.
[31] Rundle JB, Turcotte DL, Shcherbakov R, Klein W, Sammis C. Statistical physics approach to understanding the multiscale dynamics of earthquake fault systems. Rev Geophys 2003;41:1–30.
[32] Turcotte DL. Fractals and chaos in geology and geophysics. New York: Cambridge University Press; 1997.
[33] Colombo S, Main IG, Forde MC. Assessing damage of reinforced concrete beam using "*b*-value" analysis of acoustic emission signals. J Mater Civil Eng ASCE 2003;15:280–6.
[34] Rao MVMS, Prasanna Lakshmi KJ. Analysis of *b*-value and improved *b*-value of acoustic emissions accompanying rock fracture. Curr Sci 2005;89:1577–82.
[35] Lockner DA, Byerlee JD, Kuksenko V, Ponomarev A, Sidorin A. Quasi static fault growth and shear fracture energy in granite. Nature 1991;350:39–42.
[36] Carpinteri A, Lacidogna G. Damage evaluation of three masonry towers by acoustic emission. Eng Struct 2007;29:1569–79.
[37] Carpinteri A, Lacidogna G, Niccolini G. Fractal analysis of damage detected in concrete structural elements under loading. Chaos, Solitons Fractals 2009;42:2047–56.
[38] Carpinteri A, Lacidogna G, Puzzi S. From criticality to final collapse: evolution of the *b*-value from 1.5 to 1.0. Chaos, Solitons Fractals 2009;41:843–53.
[39] Aggelis DG. Classification of cracking mode in concrete by acoustic emission parameters. Mech Res Commun 2011;38:153–7.
[40] Aggelis DG, Mpalaskas AC, Ntalakas D, Matikas TE. Effect of wave distortion on acoustic emission characterization of cementitious materials. Constr Build Mater 2012;35:183–90.